
Article:
Parastesh, H., Hajirasouliha, I. orcid.org/0000-0003-2597-8200, Taji, H. et al. (1 more author) (2019) Shape optimization of cold-formed steel beam-columns with practical and manufacturing constraints. Journal of Constructional Steel Research, 155. pp. 249-259. ISSN 0143-974X

https://doi.org/10.1016/j.jcsr.2018.12.031

Journal of Constructional Steel Research 155 (2019) 249–259

Shape Optimization of Cold-Formed Steel Beam-Columns with Practical and Manufacturing Constraints

Hossein Parastesh [a,*], Iman Hajirasouliha [b], Hamed Taji [a], Alireza Bagheri Sabbagh [c]

[a] *Civil Engineering Department, University of Science and Culture, Tehran, Iran*

[b] *Department of Civil and Structural Engineering, University of Sheffield, UK*

[c] *School of Engineering, University of Aberdeen, UK*

Abstract

This study aims to present a practical method for optimization of symmetric cold-formed steel (CFS) beam-column members using Genetic Algorithm (GA). To eliminate impractical cross-section shapes from the optimization results, a range of manufacturing and construction constraints are incorporated into the optimization process. Axial forces are applied with different eccentricities (0 to 30 mm) to cover the full spectrum of beam-column actions from pure axial compression to pure bending. The effect of element length on the optimization results is investigated by using short, intermediate and long beam-column members. A total of 132 beam-columns with different cross section shape complexity (4 to 12 rollers/nodes and 1 to 3 lips) are optimized. The compression and bending moment strengths are obtained based on direct strength method (DSM) using CUFSM software by accounting for local, distortional and global buckling modes. The results show that using more complex shapes does not necessarily lead to better design solutions. Increasing the eccentricity generally leads to more spread optimum sections particularly when distortional buckling is the predominant mode in short and intermediate-length beam-columns. In cases where local and global buckling modes govern the design, however, less spread sections with higher turn angles generally provide higher strength capacities. With the variation of eccentricity, the ultimate strength of optimum beam-column sections normalised by the strength of a reference lipped-channel are in the range of 110-163%, 128-194% and 160-222% for short, medium and long members, respectively. The results of this study, should prove useful in more efficient design of CFS beam-column elements in practice.

Keywords: Cold-formed steel; Shape optimization; Genetic Algorithm; Beam-columns; Buckling modes

* Corresponding author. Email: Parastesh@usc.ac.ir

1. Introduction

Light steel frames (LSF) made of cold-formed steel (CFS) sections are growing popularity in construction industry to provide cost-effective and sustainable buildings due to the advantages such as ease of off-site manufacturing and faster construction, light weight and high flexibility in obtaining various cross-sectional shapes, and highly adaptable manufacturing process [1]. A range of CFS cross-section shapes can be manufactured from simple C channel sections to more complex shapes with multiple segments, stiffeners and lips [2]. The use of more complex CFS sections aims to achieve increased local buckling resistance and improved load-deformation characteristics of CFS elements. This motivates research on shape optimization of CFS sections for different structural elements and various loading conditions. Previous studies have demonstrated that CFS beam and column members are mainly affected by local, global and distortional modes of buckling, and therefore, their yielding strength cannot be generally reached due to the premature failure modes [3-5]. This highlights the importance of using optimization tools to increase the buckling resistance of CFS elements and develop more economic design solutions with higher strength-to-weight ratios.

Leng et al. [6] investigated the application of different optimization tools to maximize the compressive strength of CFS open cross-sections. They determined local, distortional and global buckling loads using the open source CUFSM software [7, 8] and then adopted the Direct Strength Method (DSM) [9] to estimate the nominal compressive strength of the CFS elements. Ostwald and Rodak [10] presented a method for multi-criteria optimization of CFS beams with open sections subjected to various loading conditions. In their work, the concept of Pareto optimality was used to solve the multi-criteria optimization problem, in which the cross-section area and deflection of beams were considered as the main objective functions. In another relevant study, Moharrami et al. [11] used a combination of Genetic Algorithm (GA) and Gradient Descent Optimization (GDO) to investigate the effect of different boundary conditions on the optimum design of CFS elements under axial loads. To provide more practical design solutions, Leng et al. [12] adopted a simulated annealing (SA) algorithm to optimize CFS columns subjected to predefined manufacturing constraints. Maderia et al. [13] also investigated the optimal shape of CFS columns sing a multi-objective optimization method. In their study, the objective functions were the maximum local-global buckling strength and the maximum distortional buckling strength of the sections calculated based on DSM [9].

Ma et al. [14] employed GA to optimize the shape of CFS channel sections in compression or bending by adding double-fold lips, inclined lips and triangular stiffeners based on the effective

width method in Eurocode 3 [15, 16]. They also investigated the influence of the shift of the neutral axis on the optimization results of the CFS compression sections with different member lengths. Using the same design concept, Ye et al. [17, 18] utilized Particle Swarm Optimization (PSO) to optimize CFS beam elements for maximum bending capacity. The results of their study indicated that optimized folded-flange sections can provide up to 57% higher bending capacity compared to standard optimized shapes with the same amount of structural material. In a follow-up study, Ye et al [19] developed optimum CFS beam sections with maximum energy dissipation capacity through a shape optimization framework, which links the PSO algorithm to detailed finite element (FE) models. It was concluded that, compared to commercially available lipped channels, optimized cross-sectional shapes can dissipate up to 60% more energy through plastic and yielding deformations, and therefore, provide better design solutions for seismic applications.

As discussed above, the focus of the CFS optimization research to date has been on isolated beam and column members, in which the axial load-bending moment interaction has not been considered. However, the application of CFS as beam-column members, for instance in CFS moment-resisting frame systems [20], requires bending-compression interaction effects to be incorporated in the design and optimization process. While the effect of bending moment-axial force interaction on optimal design of hot rolled members has been investigated in the past (e.g. [21]), this can be a challenging task for CFS elements due to their complex behavior affected by different local and global buckling modes. In this study, for the first time, an efficient optimization framework is proposed to optimize CFS beam-column members by taking into account the axial load-bending moment interaction effects. A Genetic Algorithm (GA) is adopted to maximize the ultimate capacity of short, intermediate and long length beam-column elements, while a wide range of practical end-use and manufacturing constraints (described in Section 3) are considered to improve the feasibility of the optimized sections. To define the objective function, a new design formulation is developed based on DSM [9] to take into account the axial compression force-bending moment interactions calculated by using CUFSM software [8]. The proposed optimization framework is then used to optimize 132 beam-columns to investigate the influence of different design parameters and provide practical recommendations for more efficient design of CFS beam-column elements.

2. The Objective Function

This section provides detailed information about the proposed optimization framework including design variables (cross-section components), practical and end-use constraints, and the adopted strength calculation method and fitness function.

2.1 Cross-section components

Fig. 1 illustrates a typical beam-column section consisting of finite strips with intersections at the nodes, which represent the location of the rollers used to fold the cross-section. The cross-section is considered to be on the XY plane with the origin of the coordinate system at the tip of the first strip. All CFS beam-column cross-sections are assumed to be manufactured from a coil sheet with a fixed width and thickness to use the same amount of structural material. As can be seen in Fig. 1, the width of the strips, L_i, and the turn-angles in the counterclockwise direction, θ_i, can define the whole geometry of the section, and therefore, are considered as the main design variables in the optimization process.

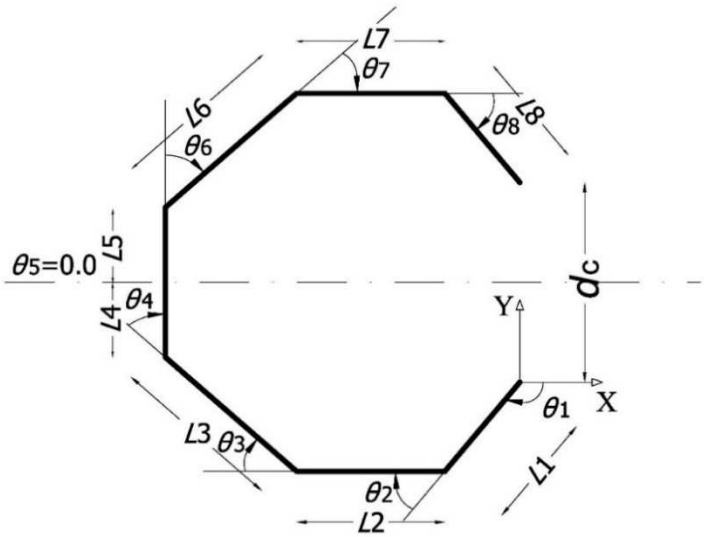

Fig. 1. Definition of design variables in constrained shape optimization

In this study, the number of rollers (n_{roll}) is assumed an even number between 4 and 12. As mentioned before, the non-zero turn-angles represent the locations of the rollers to form a symmetric section. For the symmetric cross-sections identified as above, the design variables are defined for half of the section with the axis of symmetry positioned at the mid-height parallel to the X-axis (see Fig. 1). The total width of the coil (d) is equal to the sum of all strips:

$$d = \sum_{i=1}^{2n} L_i \tag{1}$$

where n is the number of half cross-section strips calculated by:

$$n = n_w + n_f + n_l \tag{2}$$

The half cross-section design variables n_l, n_f and n_w are the number of strips corresponding to the lip, flange and web, respectively. Subsequently, the number of required rollers n_{roll} can be

calculated by:

$$n_{roll} = 2n - 2 \tag{3}$$

For instance, based on the above definitions, the design variables of the example section shown in Fig. 1 are $n_{roll} = 6$, $n_l = 1$, $n_f = 1$, $n_w = 2$ *and* $n = 4$.

To identify the location of the i^{th} strip, the following labels are utilized in this study:

$$\begin{cases} \text{L} & \text{if } i \leqslant n_l \\ \text{F} & \text{if } n_l + 1 \leqslant i \leqslant n_l + n_f \\ \text{W} & \text{otherwise} \end{cases} \tag{4}$$

where L, F and W denote lip, flange and web strips, respectively, as shown in Figure 2. The same notations have been used by Leng et al. [12] for shape optimization of CFS columns.

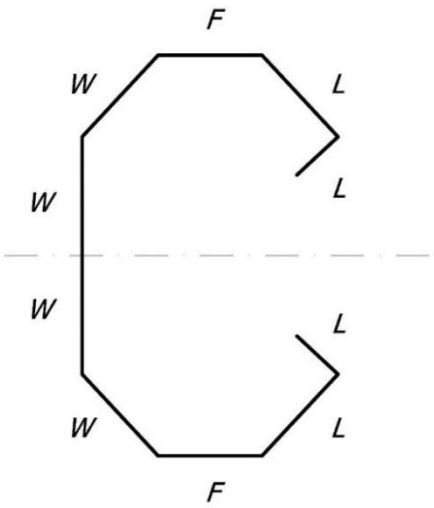

Fig. 2. Identification of lip, flange and web strips

2.2. Fitness function

In this study, DSM [9] is adopted to determine the nominal compression capacity (P_n) and the bending strength (M_n) of CFS beam-column elements based on the minimum of their local (P_{nl}, M_{nl}), distortional (P_{nd}, M_{nd}) and global (P_{ne}, M_{ne}) buckling loads as follows:

$$\begin{cases} P_n = \min\left\{P_{nl}, P_{nd}, P_{ne}\right\} \\ M_n = \min\left\{M_{nl}, M_{nd}, M_{ne}\right\} \end{cases} \tag{5}$$

The critical elastic local, distortional and global compression loads (P_{crl}, P_{crd}, P_{cre}) and bending moments (M_{crl}, M_{crd}, M_{cre}) are calculated by using CUFSM software [8] and fed into DSM equations to obtain the buckling loads in Eq. (5). The compression-bending moment design interaction has been adopted from [22] as given in the equation below after rearranging the original equation (see Appendix A):

$$\left(\frac{-\Omega_c^2 M_{\mathrm{nx}}}{P_{\mathrm{E}}}\right).P^2+\left(\Omega_c M_{\mathrm{nx}}+\Omega_{\mathrm{b}} P_n C_{\mathrm{mx}}.e+\frac{P_{\mathrm{n}}.M_{\mathrm{nx}}\Omega_c}{P_E}\right)P-P_{\mathrm{n}}.M_{\mathrm{nx}}=0 \tag{6}$$

In the above equation, e is the eccentricity of the design axial load, which produces the required bending moment (M=$P.e$). Using an axial load eccentricity factor provides a practical way to present the code design equations for optimization of beam-column elements. In this case, the ultimate capacity of the member (P) can be considered as the objective function of the optimization problem as follows:

$$\begin{cases}\text{maximize } \{p(\mathrm{x})\}\\ \text{Subjected to: } g_{\mathrm{i}}(\mathrm{x})\leqslant 0 \quad \text{for } i=1,2,\ldots,N\end{cases} \tag{7}$$

where N is the number of design constraints as defined in the following section.

3. Manufacturing and End-Use Design Constraints

To obtain optimized beam-column elements with feasible and practical cross-sections, various end-use and manufacturing geometrical constraints are considered in this study. Practical limitations on rounded corner turn-angles and minimum strip width (e.g. for ease of manufacturing process and connection of the elements to flooring or walling panels) are incorporated in the beam-column optimization problem as end-use constraints. The sections are also designed to have symmetrical shapes that can be used for back-to-back sections, have open sections suitable for cold-rolling manufacturing process and satisfy minimum utility pass-through allowance as will be discussed in more detail below.

Considering the axis of symmetry parallel to the X-axis (see Fig. 1) and assuming n as the number of strips in half of the section, the symmetry constraint equation is given by [12]:

$$\theta_{2\mathrm{n}-\mathrm{i}+} = +\theta_{i+1} \quad \text{for} \quad i=1,2,\ldots,\frac{n_{\mathrm{roll}}}{2} \tag{8}$$

The utility pass-through constraint allows the building utilities to be positioned inside the roofing system through the CFS webs. To provide this, a minimum opening distance (d_c in Fig. 1) of 25.4 mm has been considered as suggested by Leng et al. [12].

In addition, to facilitate perforation and installation of the utilities, the two middle web strips are considered to be perpendicular to the flanges (i.e. X-axis in Fig. 1) to form a flat web. As a result, the turn-angle at the mid-point is always zero while the number of rollers (or bending points) should be even. Considering the geometry of the sections, θ_n and θ_{n+1} can be easily obtained from the following equations [12]:

$$\begin{cases} \theta_n = \begin{cases} -\frac{\pi}{2} & \text{if} \quad n_w = 1 \\ -\frac{\pi}{2} - \sum_{n_L+n_F+1}^{n-1} \theta_i & \text{otherwise} \end{cases} \\ \theta_{n+1} = 0 \end{cases} \tag{9}$$

It should be noted that Eq. (9) implies that θ_n and θ_{n+1} are dependent design variables. To enable the attachment of flooring or walling panels to the CFS sections, the flanges of the beam-column sections are designed to be parallel to the X-axis with a minimum width of 25.4 mm. These conditions can be achieved by satisfying Eqs. (10) and (11), which also imply that the flange turn-angle is a dependent variable. To obtain feasible shapes, the Y coordinate of the lower flange strip has been assumed to be less than the other strips.

$$L_F = L_{n_L+1} \geq 25.4 \text{ mm} \tag{10}$$

$$\theta_{n_L+1} = -\pi - \sum_{i=1}^{n_L} \theta_i \tag{11}$$

For the lip stiffeners and the non-vertical components of the web, a minimum strip width constraint of 6.35 mm is used to provide sufficient distance between the roller points in the cold-rolling process as recommended by Leng et al. [12].

To avoid expensive manufacturing process, in this study the maximum number of rollers has been capped to 12. As discussed before, the number of rollers (or bending points) should be also an even number to satisfy the symmetry and utility pass-through allowance constraints. Considering Eqs (2) and (3), the maximum number of lip strips ($n_{l,\max}$) can be equal to 1, 2 and 3 when the number of half cross-section strips (n) is 3, 4 and greater than 5, respectively.

Open section and rounded corner constraints were also applied to avoid overlapping of the cross-sectional strips and sharp corners, respectively. The rounded corner radius-to-thickness ratio of less than 5 has been assumed, which is double the limit specified in AISI-S100-07 [9]. Finally, to facilitate connecting double back-to-back sections, the X coordinate of the central strip on the web was forced to be less than the other strips.

4. Implementation of the GA

The objective of the optimization procedure is to maximize the ultimate capacity of the CFS beam-columns under the combined effects of axial load and bending moment, while also satisfying the design constraints explained in the previous section. A Genetic Algorithm (GA) approach was adopted to solve this complex optimization problem. GA is a random search method based on principles of natural evolution, in which a population of candidate solutions is evolved through special selection rules to optimize the fitness function (optimization target) during the evolution process [23-25]. To achieve this, a primitive population of chromosomes is first created, each representing a possible answer to the problem. These chromosomes are then evaluated based on the optimization goal, and the best design solutions (i.e. with higher fitness values) have a greater chance of re-producing the problem answers. The formulation of the chromosome evaluation function is key to achieve convergence towards a global optimal answer and to reduce the computational cost.

Fig. 3 illustrates the flowchart of the process to create feasible cross-sections by implementing the design constraints used in this study. In the adopted method, the number of rollers (n_{roll}), lip strips (n_l) and flange strips (n_f) for the half cross-section are first specified. The number of web strips (n_w) and the total number of strips in the whole cross-section ($2n$) are then calculated by using Eqs. (2) and (3). Subsequently, two design variable vectors of length and turn-angle are randomly generated for half of the cross-section by considering the minimum and maximum bounds discussed in Section 3. Since the cross-sections are considered to be symmetric, these variable vectors can represent the whole cross-section. After completing the constraint checks, DSM [9] is adopted to calculate the compression and bending strength of the feasible beam-column cross-sections as explained in Appendix A.

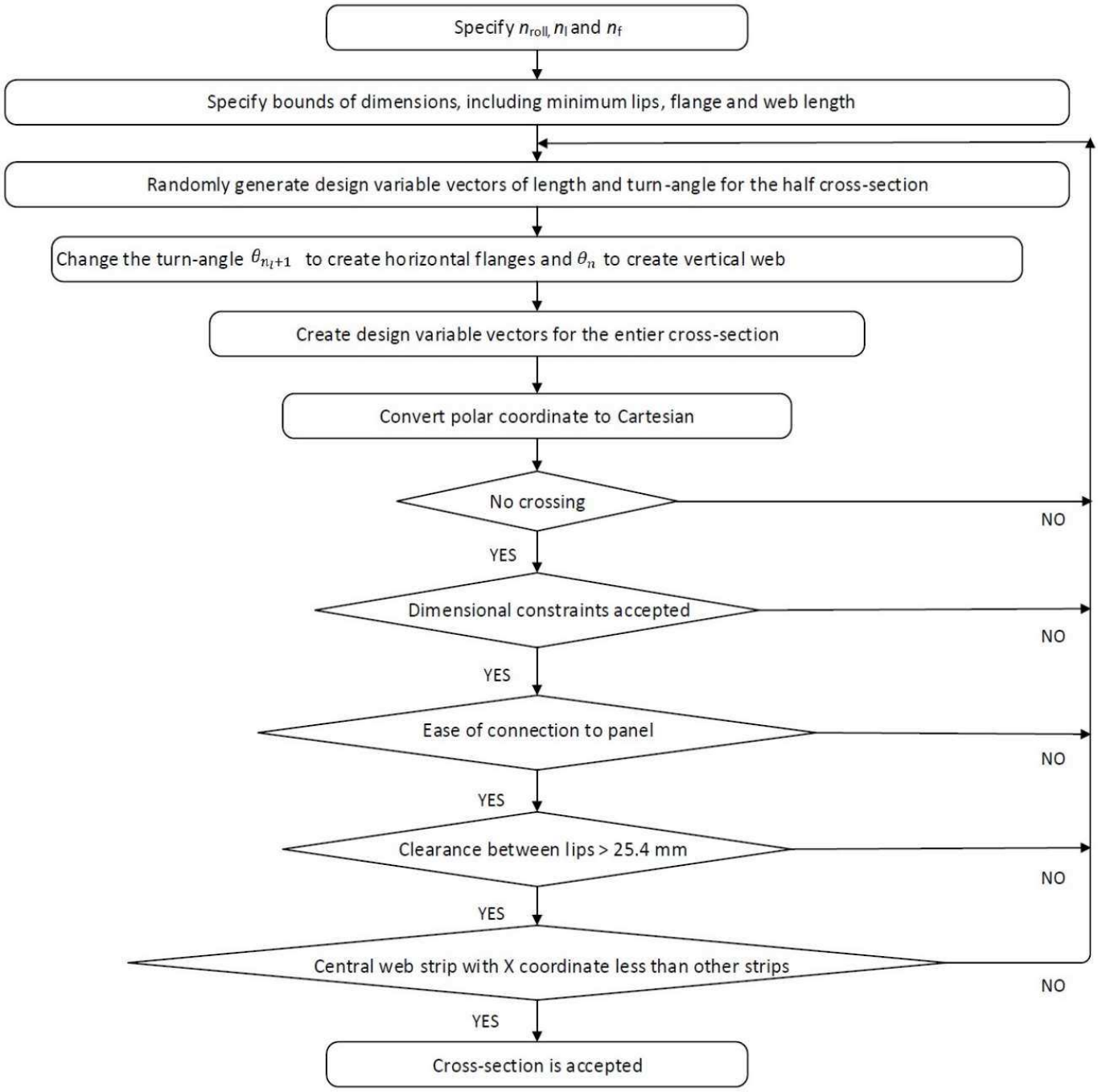

Fig.3. Flowchart of feasible cross-section creations

A summary of the Genetic Algorithm used in this study is given in Fig. 4. The analysis was started with a population size of 80 individuals (n_{pop}=80) and was run for 100 generations (n_{max}=100). The mutation rate in the optimization process was considered to be r_m =0.02. Based on repeated runs with 20, 50, 80 and 100 generations, the optimum solution was not found to change significantly past 50 generations. The "roulette wheel" method was used to select parents, while a single point crossover was used to exchange variable design information vectors between two parents. The crossover and mutation operators were applied on both length variable and turn-angle variable vectors.

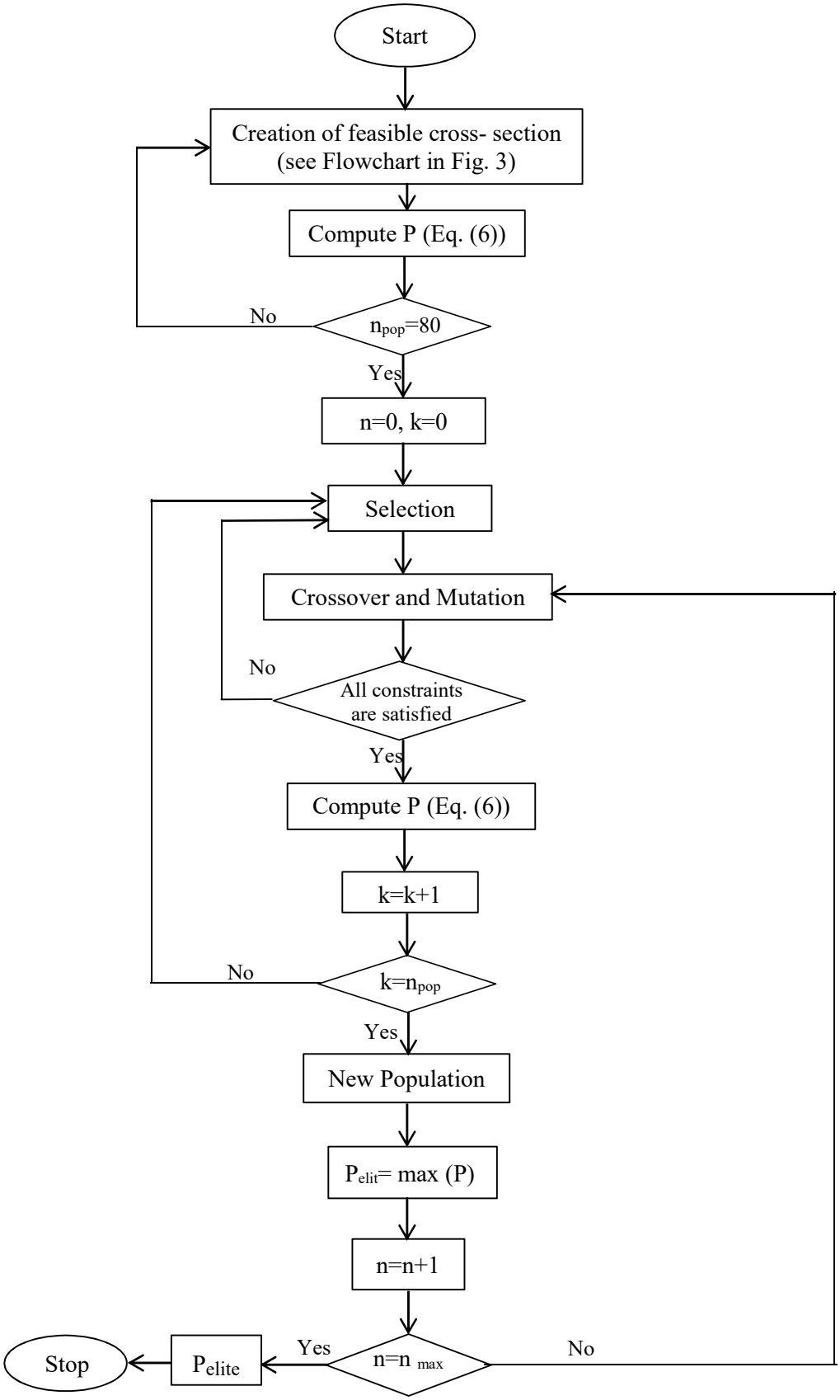

Fig.4. Flowchart of the adopted GA optimization process

5. Optimization Results

The proposed framework was used to optimize the CFS beam-columns with short, intermediate and long lengths (1000, 2000, and 3000 mm, respectively) aiming for the maximum ultimate capacity incorporating the aforementioned practical and manufacturing constraints. The total width and the thickness for the steel plate were d=320 mm and t=1 mm, respectively. The modulus of elasticity of E = 210 GPa and the yield stress of F_y = 350 MPa were used as a typical steel material. The beam-column members were subjected to axial compressive loads with eccentricities of e vary from 0 to 30 mm (with 10 mm intervals) to create different levels of bending moment about the X-axis (see Fig. 3 for the reference shape). The cross-sectional shapes were based on using variations number of rollers (even numbers from 4 to 12) and lips (1, 2 or 3). The choice of the design shapes was to increase the cross-section complexity through increasing the number of rollers and lips. Therefore, only one lip was considered for the sections made with four rollers, up to two lips were used for the sections made with six and eight rollers, and lastly, up to three lips were used for the sections with ten or twelve rollers. This creates eleven cross-sectional shapes, which can be identified by a two-digit number standing for the number of rollers and the lip strips. For example, cross-section 4-1 represents a section with four rollers and one lip strip as shown in Table 1.

The following subsections present the optimization results for three sets of 1000, 2000 or 3000 mm long beam-column members, each with four eccentricity levels (e = 0, 10, 20 and 30 mm) and eleven design shapes as explained above. These generate a total of 132 independent non-linear optimization problems. Fig. 5 shows the dimensions of a standard lipped channel section used as a reference in this study.

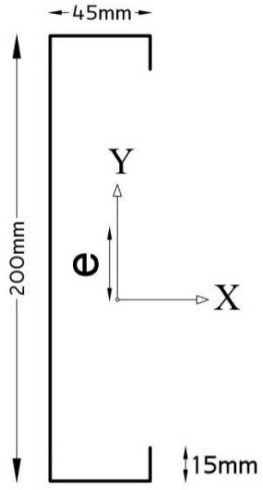

Fig. 5. Reference standard lipped channel section

Table 1. Optimized cross-sections for 1000 mm long beam-columns

design shape	*e* =0	*e* =10	*e* =20	*e* =30
4-1	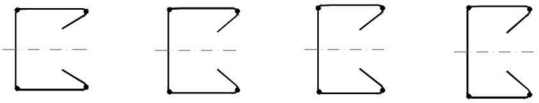			
6-1	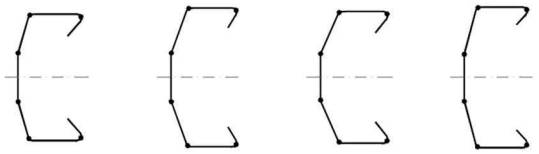			
6-2	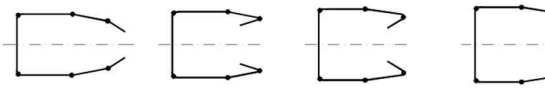			
8-1	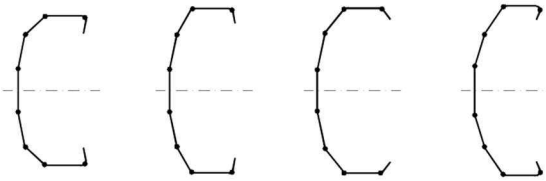			
8-2	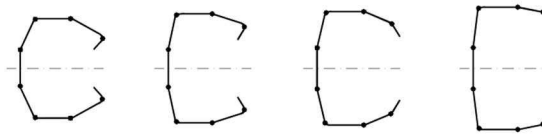			
10-1	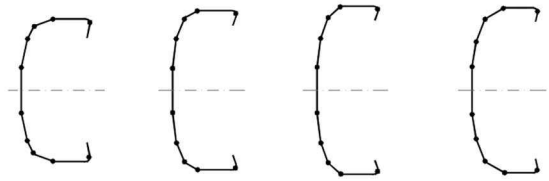			
10-2	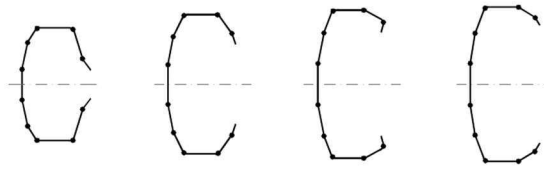			
10-3	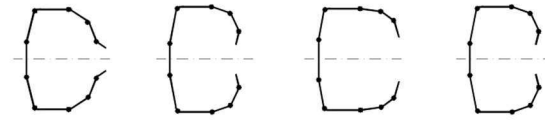			
12-1	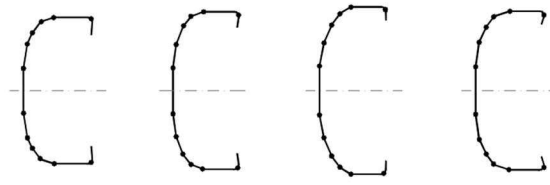			
12-2	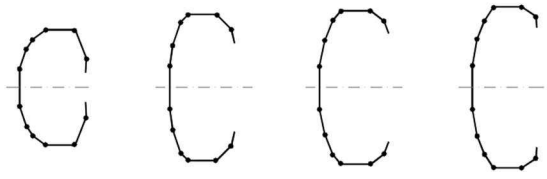			
12-3	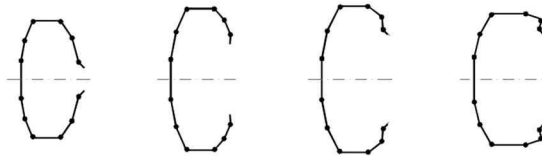			

5-1. Results for short beam-columns

Table 1 illustrates the optimal cross-sections obtained for the short (1000 mm long) beam-columns with different design shapes and eccentricity levels. For better comparison, Table 2 also presents the corresponding warping coefficient (C_w), the nominal axial compression and bending moment normalized by the yielding axial force and moment (P_n/ P_y and M_{nx} / M_{yx}), and the ultimate capacity of the beam-column member P (objective function) calculated from Eq. (6). For each element, the dominant buckling modes for the axial compression and bending moment are calculated through elastic buckling analysis using CUFSM [8] and denoted by the letter "l", "d" and "g" for local, distortional and global buckling modes, respectively. The last column in Table 2 shows the ratio of the optimum beam-column strength to that of the standard lipped channel section (Fig. 5) with the same plate width and thickness. This number can be used to assess the efficiency of each optimum design solution.

Table 2. Warping coefficient, normalized nominal loads and optimized strength for 1000 mm long beam-columns with different eccentricities.

e = 0					
design shape	C_w (cm^6)	$\frac{P_n}{P_y}$	$\frac{M_{nx}}{M_{yx}}$	P (kN)	$\frac{P}{P_{ref}}$
Lipped channel	782	0.34 (l)	0.73 (l)	21.1	1
4-1	858.7	0.5032 (d)	0.6506 (d)	31.3	1.48
6-1	986	0.7405 (d)	0.7659 (d)	46.1	2.18
6-2	1093	0.6557 (d)	0.7777 (d)	40.8	1.93
8-1	1002	0.8221 (l,g)	0.8745 (d)	51.1	2.42
8-2	1817	0.8540 (d)	0.9326 (d)	53.2	2.52
10-1	1076	0.8304 (l,g)	0.8972 (d)	51.7	2.45
10-2	1921	0.8935 (l,g)	0.9856 (d)	55.6	2.63
10-3	2207	0.8897 (l,g)	1	55.3	2.62
12-1	1082	0.8311 (l,g)	0.8918 (d)	51.7	2.45
12-2	1976	0.8865 (l,g)	1	52.2	2.47
12-3	1977	0.9055 (l,g)	1	56.3	2.67
e = 20 mm					
Lipped channel	782	0.34 (l)	0.73 (l)	18.3	1
4-1	975	0.4894 (d)	0.7397 (d)	22	1.2
6-1	950	0.7134 (d)	0.7892 (d)	32.4	1.78
6-2	1041	0.6151 (d)	0.8420 (d)	25.3	1.38
8-1	908	0.8095 (l,g)	0.8898 (d)	38.2	2.09
8-2	1589	0.8196 (d)	0.9279 (d)	35.9	1.96
10-1	890	0.8180 (l,g)	0.9701 (d)	39.4	2.15
10-2	1220	0.8611 (l,g)	1	40.3	2.2
10-3	1683	0.8628 (l,g)	1	37	2.02
12-1	884	0.8059 (l,g)	0.9735 (d)	38.9	2.12
12-2	1221	0.8565 (l,g)	1	40.2	2.2
12-3	1324	0.8701 (l,g)	1	40	2.19

e = 10 mm					
design shape	C_w (cm^6)	$\frac{p_n}{p_y}$	$\frac{M_{nx}}{M_{yx}}$	P(kN)	$\frac{p}{p_{ref}}$
Lipped channel	782	0.34 (l)	0.73(l)	19.6	1
4-1	1023	0.4963 (d)	0.6817 (d)	25.7	1.31
6-1	970	0.6977 (d)	0.7900 (d)	37	1.89
6-2	831	0.6250 (d)	0.7621 (d)	29.8	1.52
8-1	906	0.8166 (l,g)	0.8711 (d)	43.6	2.22
8-2	1496	0.8533 (d)	0.9477 (d)	43.4	2.21
10-1	968	0.8277 (l,g)	0.9502 (d)	44.6	2.27
10-2	1144	0.8767 (l,g)	1	46.3	2.36
10-3	1940	0.8867 (l,g)	1	44.2	2.25
12-1	993	0.8254 (l,g)	0.9479(d)	44.4	2.26
12-2	1388	0.8754 (l,g)	1	46.2	2.36
12-3	1449	0.8844 (l,g)	1	46.1	2.35
e = 30 mm					
Lipped channel	782	0.34 (l)	0.73 (l)	17.2	1
4-1	989	0.4758 (d)	0.7644 (d)	19.5	1.13
6-1	790	0.7038 (d)	0.8073 (d)	29.3	1.70
6-2	1332	0.5867 (d)	0.8396 (d)	21.6	1.26
8-1	791	0.7793 (l,g)	0.9574 (d)	34	1.98
8-2	1283	0.8044 (l,g)	0.9370 (d)	32.7	1.90
10-1	899	0.8114 (l,g)	1	35.4	2.06
10-2	1172	0.8574 (l,g)	1	36.2	2.10
10-3	1125	0.8574 (l,g)	1	36.1	2.10
12-1	956	0.8167 (l,g)	1	35.4	2.05
12-2	1093	0.8462 (l,g)	1	36.1	2.10
12-3	1354	0.8577 (d)	1	34.6	2.01

The optimized shapes in Table 1 indicate that all the constraining requirements specified in Section 3 have been satisfied through the adopted GA optimization. A clear change of optimized shapes can be traced when eccentricity increased from 0 to 30 mm particularly in more complex sections with higher numbers of rollers (bending points) and lips. This is more evident in 8-2, 10-2, 12-2 and 12-3 section shapes showing a clear approach to more spread sections in the case of high bending moments compared to more lumped sections in pure axial compression.

The optimum ultimate strength, P, values in Table 2 indicate that, as expected, section 4-1 produces the lowest strength compared to more complex shapes having more rollers and lips. The ultimate strengths of section 4-1 with different eccentricity levels, however, are still higher than the strength of the reference lipped channel by 48, 31, 20 and 13% for the beam-columns with 0, 10, 20 and 30 mm eccentricity, respectively. This decreasing trend shows that the standard lipped channel sections are more suitable when bending moment governs the design (i.e. high eccentricity values). This conclusion is general and a similar trend is observed for the other cross sections.

It is shown in Table 2 that the maximum increase in the strength belongs to the more complex cross-section shapes. Amongst which, section 10-2 shows 163, 136, 120 and 110% higher strength than the reference standard channel section for 0, 10, 20 and 30 mm eccentricities, respectively. This reduction trend can be attributed to the change of the optimized cross-sections towards more spread shapes as the eccentricity of the load is increases. The results indicate that using more complex shapes did not necessarily lead to better design solutions. For example, it can be noted that the ultimate strengths of 10-2 sections (10 rollers and 2 lips) were generally higher than the most complex 12-3 sections (12 rollers and 3 lips) particularly at higher eccentricity levels. The only exception is for the pure axial compression case (i.e. $e = 0$), where 12-3 section reached the highest normalized strength of 167% which is slightly higher than that of the 10-2 section. As a result, 10-2 sections can be recommended as the most cost-effective design solutions for short beam-column members, with less complexity and higher strength compared to 10-3, 12-1, 12-2 and 12-3 sections.

In the calculation of nominal axial compression forces (P_n) for the optimum beam-column sections with lower number of rollers, the predominant buckling mode was always distortional buckling of the optimized sections, whilst local and global buckling modes were dominant when higher number of rollers were used (see Table 2). This can be due to the increase of the warping constant, C_w, in the more complex sections, which led to higher distortional buckling resistance for such sections. Distortional buckling, dominates the design for nominal bending moment, M_n, with the exception of the reference lipped channel section (see Fig. 5), where local buckling was the most critical mode of failure. In the more complex shapes, however, yielding bending moment

generally preceded the elastic modes of buckling.

Fig. 6 compares the optimized strength, P, and the warping constant, C_w, normalized by those of the reference lipped channel (denoted by solid and dashed lines, respectively) for the whole range of the design cross-section shapes from 4-1 to 12-3. To quantify the level of complexity of the design sections, the number of rollers and lips are added and assumed as the degree of complexity displayed in the bottom horizontal axis corresponding to the section labels shown at the top. From the strength curves, it can be noted that the more complex 6-2 section has lower strength than 6-1 section for the whole range of eccentricities. This confirms that increasing the number of the lips is not necessarily effective when the number of rollers (i.e. sectional nodes) is insufficient. In general, it is shown that the higher number of lips can be useful when the number of rollers is also increased, particularly in the case of pure axial compression (i.e. e = 0). This can be underpinned by comparing sections 10-1 and 12-2 with sections 10-3 and 12-3, respectively.

It is shown in Fig. 6 that after a sharp increase in the optimum strength values from section 6-2 to 8-1, increasing the number of rollers and lips generally results in less significant changes in the ultimate strength of the beam-column sections, particularly for high eccentricity levels. The higher number of lips; however, increases the warping constant, C_w, which can affect the dominant mode of buckling. For instance, sections 10-3 and 12-1 have the same degree of complexity as defined herein with reasonably close range of strength, but the former with higher number of lips has significantly greater C_w.

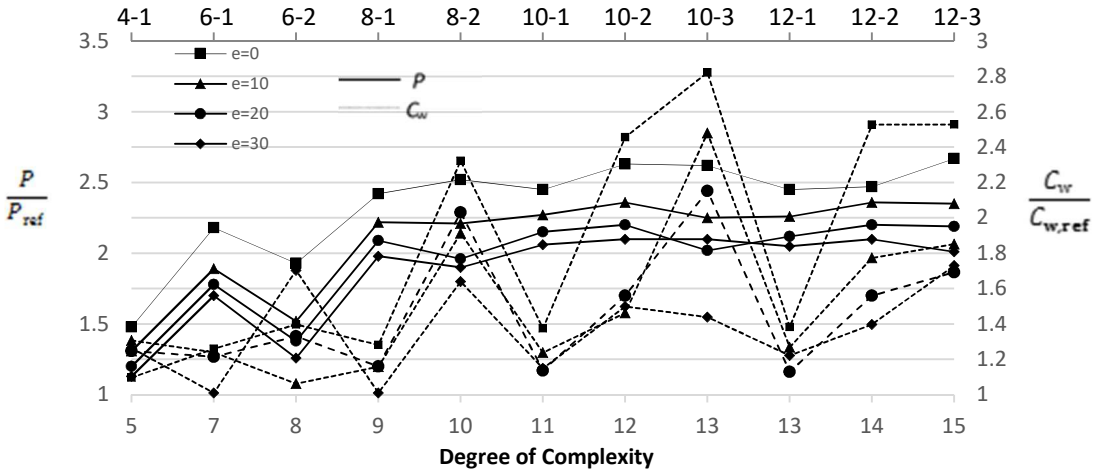

Fig. 6. Normalized strength and warping constant for 1000 mm long beam-columns

Fig. 7 shows the variation in height of the optimized sections normalized by the height of the reference section (i.e. 200 mm) as a function of load eccentricity. It can be noticed that there is a general trend towards deeper sections by increasing the eccentricity (or bending effects) as

indicated before based on the results of Table 1. It is shown in Fig. 7 that the deepest sections belong to 8-1, 10-1 and 12-1 groups (see Table 1), all of which are single-lip sections with a trend towards the shape of the reference lipped channel section. The heights of the 10-2 group sections, the most cost-effective solutions for short beam-columns as identified above, are lower than the single-lip sections but significantly higher than the two ineffectively lipped sections of 6-2 and 10-3 (see thicker dashed lines in Fig. 7).

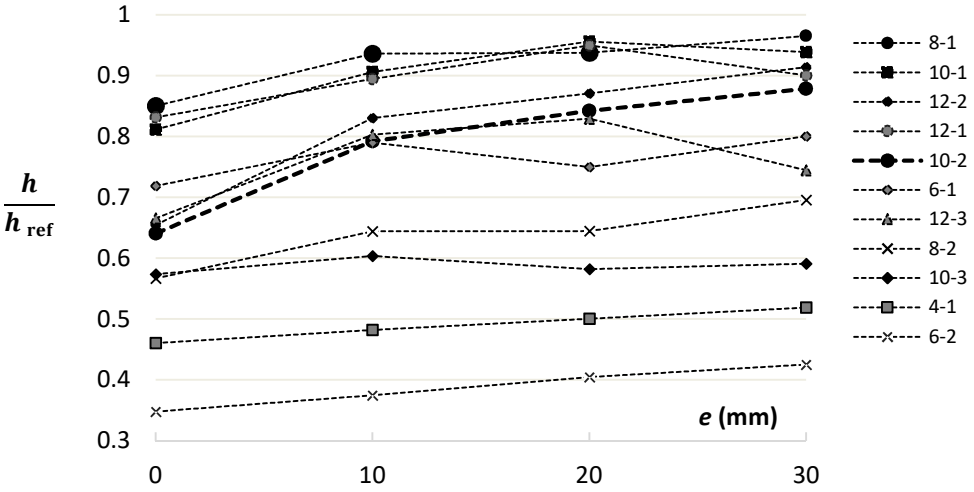

Fig. 7. Variation of normalized height with eccentricity for 1000 mm long beam-columns

5-2. Results for intermediate and long lengths beam-columns

The results obtained for the intermediate and long beam-columns with 2000 and 3000 mm lengths are presented in Tables 3 to 5 in a similar format to those of the 1000 mm long beam-columns. The results in Table 3 show a less noticeable change in the optimum design shapes due to the variation of eccentricity than those presented in Table 1 for the short-length beam-columns. The main reason for this difference is that the local and global buckling modes govern the bending moment design in the intermediate and long beam-columns (particularly in more complex sections as can be noted in Tables 4 and 5) as opposed to the predominant distortional buckling or yielding failure modes in short beam-columns. As a result, cross-section shapes with larger turn-angles between the strips and higher moment of inertia about their principle axes can respectively provide higher local and global buckling resistances. The larger turn-angles can also lead to a higher stiffening effect for the adjacent strips, and therefore, result in a higher local buckling resistance.

Table 3. Optimized cross-sections for 2000 mm and 3000 mm long beam-columns

design shape	2000 mm length				3000 mm length			
	e =0	*e* =10	*e* =20	*e* =30	*e* =0	*e* =10	*e* =20	*e* =30
4-1	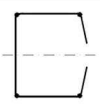	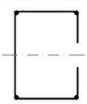	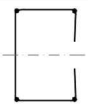				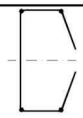	
6-1		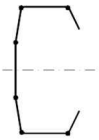	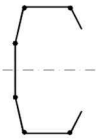					
6-2	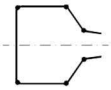	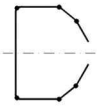	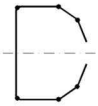	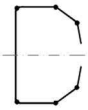	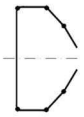	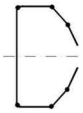	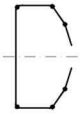	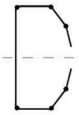
8-1								
8-2	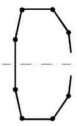		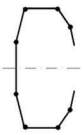		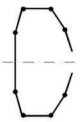	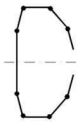		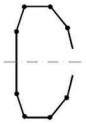
10-1								
10-2								
10-3								
12-1								
12-2								
12-3								

Table 4. Warping coefficient, normalized nominal loads and optimized strength for 2000 mm long beam-columns with different eccentricities.

$e = 0$						$e = 10$ mm					
design shape	C_W (cm^6)	$\frac{P_n}{P_y}$	$\frac{M_{nx}}{M_{yx}}$	P (kN)	$\frac{P}{P_{ref}}$	**design shape**	C_W (cm^6)	$\frac{P_n}{P_y}$	$\frac{M_{nx}}{M_{yx}}$	P (kN)	$\frac{P}{P_{ref}}$
Lipped channel	782	0.23 (l)	0.58 (l)	14.3	1	Lipped channel	782	0.23 (l)	0.58 (l)	13.4	1
4-1	1607	0.4346 (l,d)	0.6145 (d)	27	1.89	4-1	1562	0.4313 (l,d)	0.6316 (d)	22.1	1.65
6-1	1298	0.5771 (l,g)	0.6883 (d)	35.9	2.51	6-1	1313	0.5773 (l,d)	0.6838 (d)	30.4	2.27
6-2	1919	0.4671 (l)	0.8158 (d)	29.1	2.03	6-2	1994	0.4465 (l)	0.8769 (d)	23.7	1.77
8-1	1312	0.5772 (l,g)	0.7048 (d)	35.9	2.51	8-1	1261	0.5735 (l)	0.6993 (d)	30.5	2.28
8-2	1910	0.6746 (l,g)	1	42	2.93	8-2	1663	0.6647 (l,g)	0.9834 (l,g)	34.9	2.60
10-1	1351	0.5686 (l,g)	0.7134 (d)	35.4	2.47	10-1	1265	0.5709 (l,g)	0.7303 (d)	30.7	2.29
10-2	1998	0.6623 (l,g)	1	41.2	2.88	10-2	1894	0.6635 (l,g)	1	34.2	2.55
10-3	1986	0.6754 (l,g)	1	42	2.94	10-3	1788	0.6669 (l,g)	1	34.3	2.56
12-1	1329	0.5593 (l,g)	0.7520 (d)	34.8	2.43	12-1	1256	0.5569 (l,g)	0.7199 (d)	29.9	2.23
12-2	1908	0.6650 (l,g)	1	41.4	2.89	12-2	1785	0.6668 (l,g)	0.9965 (l,g)	34.5	2.57
12-3	1961	0.6746 (l,g)	1	42	2.94	12-3	1753	0.6695 (l,g)	0.9903 (l,g)	35	2.61
$e = 20$ mm						$e = 30$ mm					
Lipped channel	782	0.23 (l)	0.58 (l)	12.6	1	Lipped channel	782	0.23 (l)	0.58 (l)	11.9	1
4-1	1526	0.4249 (l,g)	0.6382 (d)	19	1.51	4-1	1437	0.4068 (l,d)	0.6439 (d)	17.2	1.44
6-1	1321	0.5702 (l,g)	0.6893 (d)	26.2	2.08	6-1	1135	0.5533 (l,g)	0.7328 (d)	24	2.02
6-2	1975	0.4442 (l)	0.8811 (d)	20.9	1.66	6-2	1947	0.4390 (l)	0.8855 (d)	18.7	1.57
8-1	1203	0.5774 (l,g)	0.7324 (d)	27.4	2.17	8-1	1144	0.5517 (l,g)	0.8144 (d)	24.8	2.08
8-2	1671	0.6465 (l)	0.9814 (d)	29.8	2.36	8-2	1490	0.6367 (l,g)	0.9610 (l,g)	27.1	2.28
10-1	1231	0.5557 (l,g)	0.7307 (d)	26.6	2.11	10-1	1176	0.5480 (l,g)	0.7765 (d)	24.3	2.04
10-2	1577	0.6529 (l,g)	0.9715 (l,g)	30.3	2.40	10-2	1601	0.6435 (l,g)	0.9749 (l,g)	26.7	2.24
10-3	1677	0.6459 (l,g)	0.9851 (l,g)	30	2.38	10-3	1495	0.6516 (l,g)	0.9599 (l,g)	27.2	2.29
12-1	1209	0.5488 (l,g)	0.7499 (d)	26.5	2.10	12-1	1142	0.5339 (l,g)	0.7869 (d)	23.9	2.01
12-2	1598	0.6510 (l,g)	0.9754 (d)	30.1	2.39	12-2	1567	0.6254 (l,g)	0.9722 (l,g)	26.8	2.25
12-3	1644	0.6464 (l,g)	0.9788 (l,g)	30.4	2.41	12-3	1596	0.6388 (l,g)	0.9736 (l,g)	27.3	2.29

Based on the results presented in Tables 4 and 5, similar conclusions can be drawn as those of the short beam-columns discussed in Section 5-1. The only difference is that for both 2000 and 3000 mm long beam-columns, section shape 8-2 is identified as the most cost-effective design solution. Compared to the standard lipped channel section, 8-2 sections with 2000 mm length provided 193, 160, 136 and 128% higher ultimate strength for 0, 10, 20 and 30 mm eccentricities, respectively. The corresponding strength improvements increased to 222, 195, 174 and 160% in 3000 mm length members. While section shape 8-2 has less degree of complexity compared to 10-3, 12-1, 12-2 and 12-3 sections, it is shown in Tables 4 and 5 that its efficiency is not very different from those sections. So this cross-section shape can be considered as the most efficient design for intermediate and long lengths beam-columns.

Table 5. Warping coefficient, normalized nominal loads and optimized strength for 3000 mm long beam-columns with different eccentricities.

design shape	C_W (cm^6)	$\frac{P_n}{P_y}$	$\frac{M_{nx}}{M_{yx}}$	P (kN)	$\frac{P}{P_{ref}}$
e = 0					
Lipped channel	782	0.13 (l)	0.35(l)	8.1	1
4-1	1807	0.3103 (l)	0.6023(d,g)	19.31	2.38
6-1	1442	0.3479 (l)	0.6375 (d)	21.6	2.67
6-2	1891	0.3149 (l)	0.8792 (d)	19.6	2.42
8-1	1452	0.3449 (l,g)	0.6391 (d)	21.5	2.65
8-2	1949	0.4200 (l,g)	0.8266 (d)	26.1	3.22
10-1	1491	0.3358 (l,g)	0.6372 (d)	20.9	2.58
10-2	1977	0.4168 (l,g)	0.8857 (l,g)	25.9	3.20
10-3	1954	0.4201 (l,g)	0.8928 (l,g)	26.1	3.22
12-1	1454	0.3370 (l,g)	0.6386 (d)	20.9	2.58
12-2	1970	0.4119 (l,g)	0.8350 (d)	25.6	3.16
12-3	1989	0.4186 (l,g)	0.8881 (l,g)	26	3.21
e = 20 mm					
Lipped channel	782	0.13(l)	0.35(l)	7.2	1
4-1	1756	0.3085 (l,g)	0.6103 (d)	14.5	2.01
6-1	1397	0.3480 (l)	0.6344 (d)	17.2	2.39
6-2	1844	0.3127 (l,g)	0.8651 (d)	15.7	2.18
8-1	1421	0.3415 (l,g)	0.6422 (d)	17	2.36
8-2	1870	0.4517 (l,g)	0.8706 (l,g)	19.7	2.74
10-1	1413	0.3343 (l,g)	0.6342 (d)	16.8	2.33
10-2	1971	0.4193 (l,g)	0.8855 (l,g)	19.7	2.74
10-3	1957	0.4224 (l,g)	0.8855 (l,g)	19.8	2.75
12-1	1453	0.3298 (l,g)	0.6382 (d)	16.6	2.31
12-2	1897	0.4058 (l,g)	0.8718 (l,g)	19.5	2.71
12-3	1969	0.4184 (l,g)	0.8843 (l,g)	19.7	2.74

design shape	C_W (cm^6)	$\frac{P_n}{P_y}$	$\frac{M_{nx}}{M_{yx}}$	P (kN)	$\frac{P}{P_{ref}}$
e = 10 mm					
Lipped channel	782	0.13 (l)	0.35(l)	7.6	1
4-1	1778	0.3103 (l)	0.6018 (d)	16.5	2.17
6-1	1354	0.3517 (l,g)	0.6386 (d)	19.3	2.54
6-2	1933	0.3143 (l)	0.8783 (d)	17.4	2.29
8-1	1459	0.3454 (l,g)	0.6358 (d)	19	2.50
8-2	1918	0.4215 (l,g)	0.8817 (l,g)	22.4	2.95
10-1	1411	0.3325 (l)	0.6357 (d)	18.4	2.42
10-2	2104	0.4244 (l,g)	0.8938 (l,g)	22.5	2.96
10-3	1943	0.4244 (l,g)	0.8852 (l,g)	22.5	2.96
12-1	1575	0.3261 (l)	0.6398 (d)	18	2.37
12-2	1973	0.4100 (l,g)	0.8851 (l,g)	21.9	2.88
12-3	1988	0.4211 (l,g)	0.8876 (l,g)	22.4	2.94
e = 30 mm					
Lipped channel	782	0.13(l)	0.35(l)	6.8	1
4-1	1688	0..3049 (l)	0.6189 (d)	13	1.91
6-1	1371	0.3516 (l)	0.6346 (d)	15.8	2.32
6-2	1854	0.3127 (l)	0.8664 (d)	14.4	2.12
8-1	1408	0.3388 (l,g)	0.6363 (l,g)	15.4	2.26
8-2	1907	0.4172 (l,g)	0.8776 (l,g)	17.7	2.60
10-1	1145	0.3431 (l,g)	0.6461 (d)	15.6	2.29
10-2	1826	0.4089 (l,g)	0.8566 (l,g)	17.7	2.60
10-3	1885	0.4147 (l,g)	0.8726 (l,g)	17.7	2.60
12-1	1439	0.3223 (l,g)	0.6546 (d)	15	2.20
12-2	1764	0.3846 (l,g)	0.8553 (l,g)	17.1	2.51
12-3	1994	0.4057 (l,g)	0.8892 (l,g)	17.4	2.56

Fig. 8 shows the variation of the normalized strength and warping constant of the 2000 and 3000 mm long beam-columns with different design shapes as a function of degree of complexity as previously defined. It can be observed that P and C_w curves corresponding to the more complex sections with higher number of rollers (section 8-1 onwards) follow a similar trend for the whole range of the eccentricities. Unlike the results obtained for the short columns (see Fig. 6), both P and C_w for intermediate and long columns are noticeably increased by increasing the number of lips, particularly from a single-lip section to a double-lip section. Increasing the number of lips from two to three, however, does not result in a significant improvement in the ultimate strength of the optimum sections. Amongst the less complex sections with lower number of rollers, section 6-1 shows higher strength than section 6-2, though the warping constant of section 6-2 is higher than that of section 6-1. These reverse trends in the strength and warping constant curves is observed in 4-1 to 8-1 range of beam-column sections. This again emphasizes the previous conclusion that the

higher number of lips is not necessarily effective for the sections with insufficient number of rollers (or bending points). Based on the results of this study, in general, minimum 8 rollers are required for the sections with more than one lip.

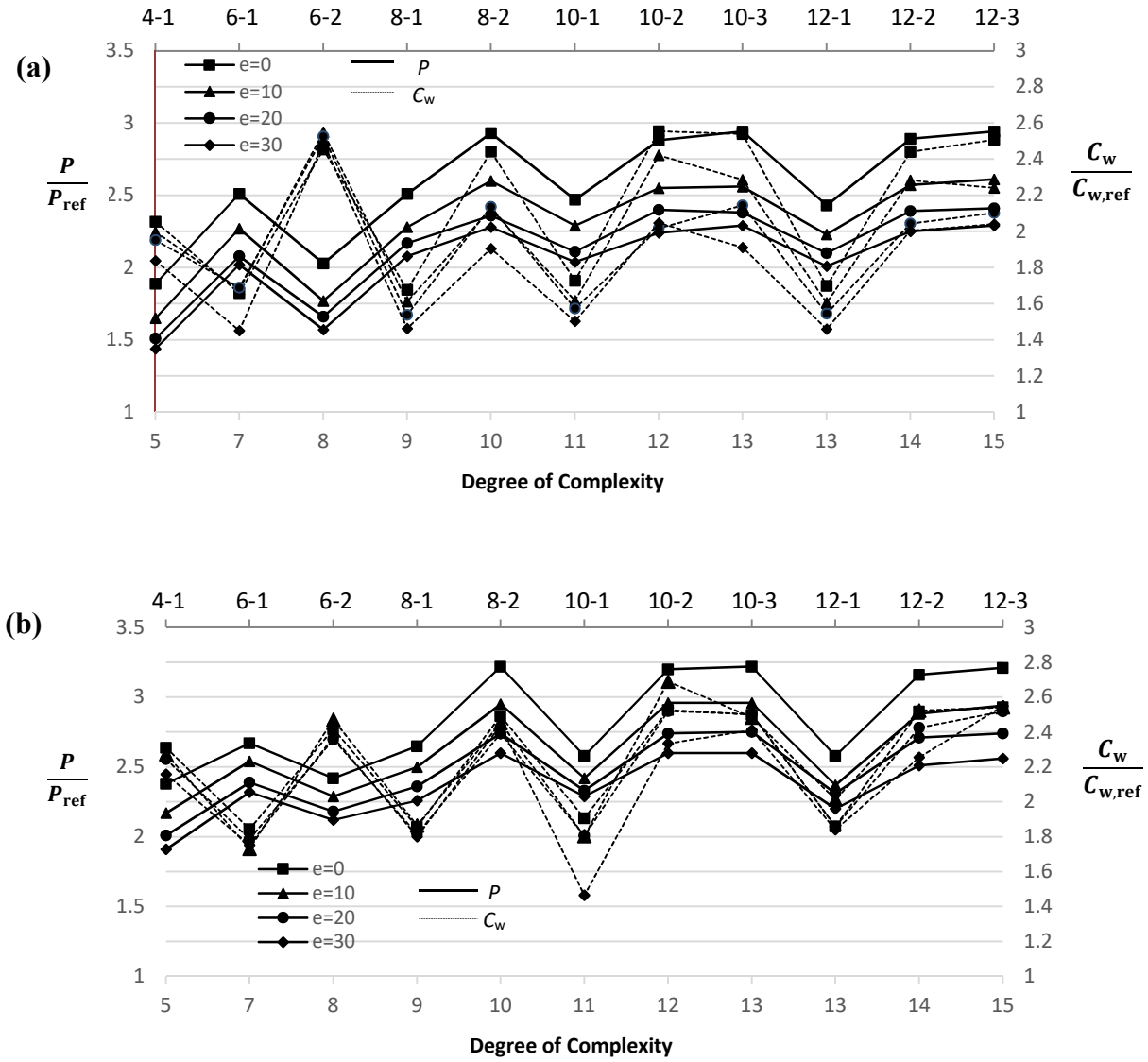

Fig. 8. Normalized strength and warping constant for (a) 2000 mm and (b) 3000 mm long beam-columns

The normalized heights of the optimum intermediate and long beam-column sections with different cross-section shapes are compared in Figs. 9 (a) and 9 (b), respectively, as a function of load eccentricity. In general, the results follow a similar trend as the short beam-columns (see Fig. 7). However, by increasing the load eccentricity a less significant increase in the height of the optimum sections is observed in the intermediate and long beam-columns (less than 15%). This can be attributed to their tendency to remain as a lumped section with larger turn-angles between the strips as explained before. Similar to the short beam-columns, the deepest shapes belong to single-

lip 6-1 to 12-1 section groups. The height of section 8-2, the most cost-effective solution for intermediate and long beam-columns as identified above, falls between that of single-lip 6-1 to 12-1 sections and the ineffective 4-1 and 6-2 sections (see thicker dashed line in Fig. 9).

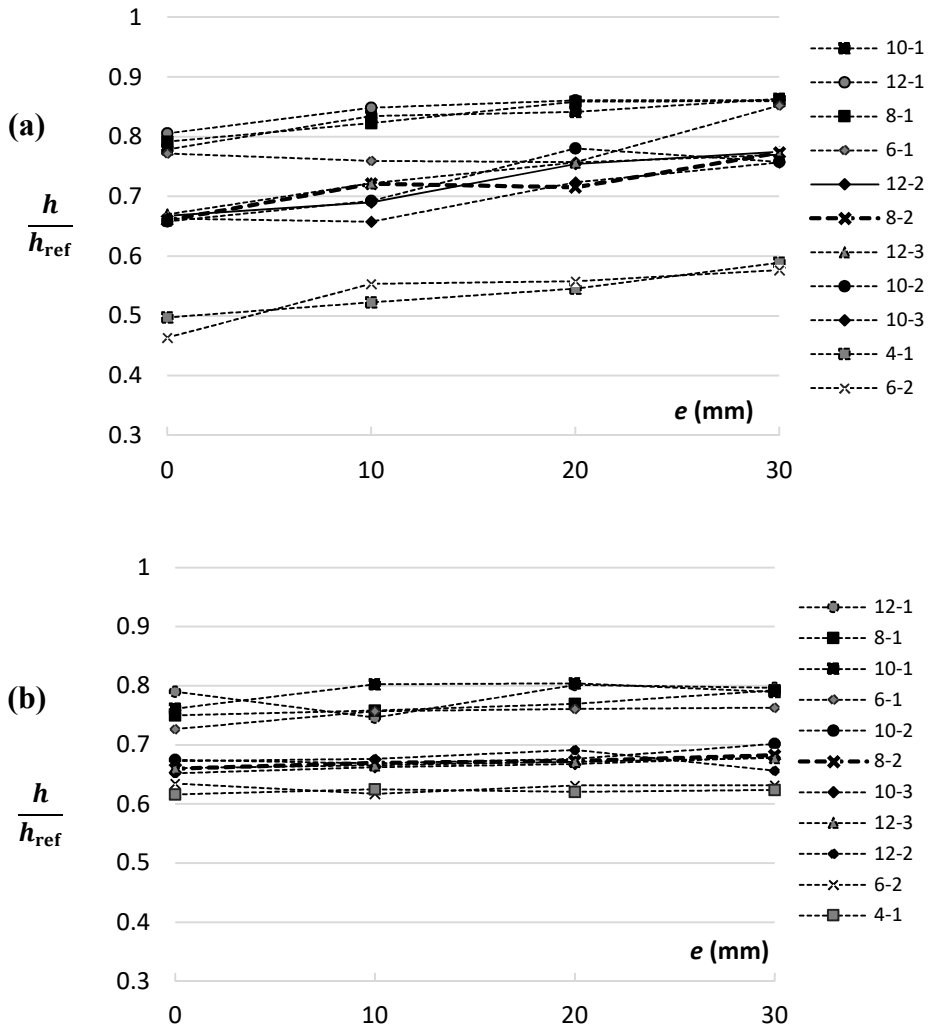

Fig. 9. Variation of normalized height with eccentricity for (a) 2000 mm and (b) 3000 mm long beam-columns

6. Summary and Conclusions

An efficient optimization framework was developed based on Genetic Algorithm (GA) to optimize the cross-section shape of cold-formed steel (CFS) beam-column elements by taking into account a wide range of practical and manufacturing constraints. The compression and bending moment strengths of the members were obtained using direct strength method (DSM) by accounting for local, distortional and global buckling loads. Three sets of short, intermediate and long beam-columns with 1000, 2000 and 3000 mm lengths were considered with axial compression loads applied with eccentricity magnitudes of e = 0, 10, 20 and 30 mm to cover the full spectrum of beam-column actions. In total 132 beam-columns were optimized using eleven different cross-

section shapes (4 to 12 rollers/nodes and 1 to 3 lips), which created a range of practical sections with different sectional complexity.

It was shown that, for the same amount of material, the optimized sections lead to significantly higher strength values compared to the reference standard lipped channel section for the whole range of length and eccentricity levels, while they satisfied all the geometric end-use and manufacturing design constraints. A general trend was observed in the shape of the optimized beam-column cross-sections, where the optimum solutions changed from lumped to more spread shapes as the load eccentricity increased. It was discussed that the shape of the optimum sections depends on the critical buckling modes, such that when local and global buckling modes are dominant (mainly in intermediate and long columns), lumped sections with higher turn-angles provide higher strength capacities.

It was shown that increasing the complexity of CFS sections does not necessarily lead to better design solutions. Especially increasing the number of lips does not increase the capacity of the beam-column sections when the number of rollers (or bending points) is insufficient. Based on the results, sections 10-2 and 8-2 were identified as the most cost-effective design solutions for short and intermediate to long beam-columns, respectively, by providing a balance between efficiency and complexity. With variation of the load eccentricity, using the suggested optimum cross sections could increase the capacity of the members in the range of 110-163%, 128-193% and 160-222% for short, intermediate and long members, respectively, compared to the reference standard lipped channel section. Therefore, the results of this study should prove useful for more efficient design of CFS beam-column members in practical applications.

References

[1] Schafer BW (2011) “Cold-formed steel structures around the world”. Steel Construction,4(3):141–9.

[2] Davies JM (2000) “Recent research advances in cold-formed steel structures”, Journal of Constructional Steel Research; 55:267-288.

[3] Ye J, Hajirasouliha I, Becque J (2018) “Experimental investigation of local-flexural interactive buckling of cold-formed steel channel columns”, Thin-Walled Structures, 245-258.

[4] Ye J, Mojtabaei SM, Hajirasouliha I (2018) “Local-flexural interactive buckling of standard and optimised cold-formed steel columns”, Journal of Constructional Steel Research; 144:106-118.

[5] Mojtabaei SM, Kabir MZ, Hajirasouliha I, Kargar M (2018) “Analytical and experimental study

on the seismic performance of cold-formed steel frames", Journal of Constructional Steel Research; 143:18-31.

[6] Leng J, Guest JK, Schafer BW (2011) "Shape optimization of cold-formed steel columns", Thin-Walled Structures; 49(12):1492–503.

[7] Li Z, Schafer BW (2010) "Buckling analysis of cold-formed steel members with general boundary conditions using CUFSM: conventional and constrained finite strip methods." Proceedings of the 20th Int;l. Spec. Conf. on Cold-Formed Steel Structures, St. Louis, MO.

[8] Schafer BW. User's manual and tutorials of CUFSM 3.12; 2010.

[9] American Iron and Steel Institute (AISI S100-07 w/S2-10 ed.). North American specification for the design of cold-formed steel structural members, 2007 edition with supplement 2, Washington, DC.

[10] Ostwald M, Rodak M (2013) "Multicriteria optimization of cold-formed Thin-walled beams with generalized open shape under different loads", Thin-walled structures; 65: 26-33.

[11] Moharrami M, Louhghalam A, Tootkaboni M (2014) "Optimal folding of cold formed steel cross sections under compression". Thin-Walled Structures; 76:145–56.

[12] Leng J, Li ZH, Guest KJ, Schafer BW (2014) "Shape optimization of cold-formed steel columns with geometric end-use constraints", Thin-Walled Structures; 85(12): 271–290.

[13] Madeira JFA, Dias J, Silvestre N (2015) "Multiobjective optimization of cold-formed steel columns", Thin-walled structures; 96:29-38.

[14] Ma W, Becque J, Hajirasouliha I, Ye J (2015) "Cross-sectional optimization of cold-formed steel channels to Euro code 3", Engineering structures; 101: 641-651.

[15] CEN. Eurocode 3: design of steel structures. Part 1–1: General rules and rules for buildings. Brussels: European Committee for Standardization; 2005.

[16] CEN. Eurocode 3: design of steel structures, Part 1.3: General rules—supplementary rules for cold formed members and sheeting. Brussels: European Committee for Standardization; 2005.

[17] Ye J, Hajirasouliha I, Becque J, Eslami A (2016) "Optimum design of cold-formed steel beams using Particle Swarm Optimisation method", Journal of Constructional Steel Research; 122: 80-93.

[18] Ye J, Hajirasouliha I, Becque J, Pilakoutas K (2016) "Development of more efficient cold-formed steel channel sections in bending", Thin-Walled Structures; 101: 1-13.

[19] Ye J, Becque J, Hajirasouliha I, Mojtabaei SM, Lim J (2018) "Development of optimum cold-

formed steel sections for maximum energy dissipation in uniaxial bending", Engineering Structures; 161: 55-67.

[20] Bagheri Sabbagh A, Petkovski M, Pilakoutas K, Mirghaderi R (2012) "Development of cold-formed steel elements for earthquake resistant moment frame buildings", Thin-Walled Structures 53, 99–108.

[21] Ozbasaran H (2018) "Optimal design of I-section beam-columns with stress, non-linear deflection and stability constraints", Engineering Structures; 171: 385-394.

[22] American Iron and Steel Institute. Direct Strength Method (DSM) design guide. Washington (DC): American Iron and Steel Institute; 2006.

[23] Holland JH. Adaptation in natural and artificial systems. Ann Arbor, Michigan: University of Michigan Press; 1975.

[24] Goldberg DE. Genetic algorithms in search, optimization, and machine learning. New York: Addison-Wesley; 1989.

[25] Andre J, Siarry P, Dogonon T (2001). An improvement of the standard genetic algorithm fighting premature convergence in continuous optimization. Advances in Engineering Software; 32: 49-60.

Appendix A. Objective Function Equation

Direct strength method (DSM) has been adopted in accordance with [9] to determine the nominal axial and flexural strength of beam-column members as follows:

$$\begin{cases} P_{\mathrm{n}} = \min\left\{P_{\mathrm{nl}}, P_{\mathrm{nd}}, P_{\mathrm{ne}}\right\} \\ M_{\mathrm{n}} = \min\left\{M_{\mathrm{nl}}, M_{\mathrm{nl}}, M_{\mathrm{ne}}\right\} \end{cases} \quad \text{(A-1)}$$

where P_{nl}, P_{nd}, P_{ne} and M_{nl}, M_{nd}, M_{ne} are local, distortional and global axial and flexural buckling strengths, respectively. Given that DSM does not currently provide the interaction equation between axial compression force and bending moment, the following has been adopted from [22].

$$\frac{\Omega_{\mathrm{c}} p}{p_{\mathrm{n}}} + \frac{\Omega_{\mathrm{b}} c_{\mathrm{mx}} M_{\mathrm{x}}}{M_{\mathrm{nx}} \propto_{\mathrm{x}}} + \frac{\Omega_{\mathrm{b}} C_{\mathrm{my}} M_{\mathrm{y}}}{M_{\mathrm{ny}} \propto_{\mathrm{y}}} \leq 1 \quad \text{(A-2)}$$

where P, M_{x} and M_{y}, are respectively the axial load and bending moments about the x and y-axes as determined from conventional linear elastic analysis. M_{x} is considered equal to $P.e$ with the assumption of e representing the eccentricity in y-axis direction (no eccentricity was considered about x-axis). C_{m} is the moment gradient factor (about x or y-axes) for a simply supported beam-column. α is the moment amplification factor (about x or y-axes) given by Eq. (A-3).

$$\alpha = 1 - \frac{\Omega_c P}{P_E} \quad \text{(A-3)}$$

where P_{E} is the elastic buckling load calculated by $P_{\mathrm{E}} = \frac{\pi^2 EI}{(kL)^2}$; and $\Omega_{\mathrm{c}} = 1.8$ and $\Omega_{\mathrm{b}} = 1.67$ are safety factors for axial and flexural loads, respectively.

By rearranging Eq. (A-2) with the adoption of the inputs as above, one can obtain Eq. (A-4) which has been incorporated in the optimization framework presented in this paper using P as the objective function.

$$\left(\frac{-\Omega_{\mathrm{c}}^2 M_{\mathrm{nx}}}{P_{\mathrm{E}}}\right).P^2 + \left(\Omega_{\mathrm{c}} M_{\mathrm{nx}} + \Omega_{\mathrm{b}} P_{\mathrm{n}} C_{\mathrm{mx}}.e + \frac{P_n.M_{\mathrm{nx}}\Omega_{\mathrm{c}}}{P_{\mathrm{E}}}\right)P - P_{\mathrm{n}}.M_{\mathrm{nx}} = 0 \quad \text{(A-4)}$$